Lipid Membranes

International Edition: DOI: 10.1002/anie.201501173
German Edition: DOI: 10.1002/ange.201501173

Amphipathic DNA Origami Nanoparticles to Scaffold and Deform Lipid Membrane Vesicles**

*Aleksander Czogalla, Dominik J. Kauert, Henri G. Franquelim, Veselina Uzunova, Yixin Zhang, Ralf Seidel, and Petra Schwille**

Abstract: *We report a synthetic biology-inspired approach for the engineering of amphipathic DNA origami structures as membrane-scaffolding tools. The structures have a flat membrane-binding interface decorated with cholesterol-derived anchors. Sticky oligonucleotide overhangs on their side facets enable lateral interactions leading to the formation of ordered arrays on the membrane. Such a tight and regular arrangement makes our DNA origami capable of deforming free-standing lipid membranes, mimicking the biological activity of coat-forming proteins, for example, from the I-/F-BAR family.*

Living cells are compartmented by lipid membranes. Their controlled and dynamic transformation is essential for numerous physiological processes, including cell motility, endocytosis, and secretion. Recently, it has become evident that specific proteins recognize and sustain such membrane transformations to organize cellular processes in space and time.[1] A major class of membrane-sculpting proteins found in all eukaryotic cells is the BAR (Bin-Amphiphysin-Rvs) domain superfamily.[2] BAR domains are highly helical dimers, which typically bind membranes through their highly charged curved interface.[3] Contrary to curvature-recognition, membrane sculpting requires high surface densities, that is, the formation of staggered coats, of the BAR subunits.[4] The propagation of membrane deformations is due to the oligomerization of BAR domains into tightly packed scaffolds held together mostly by lateral interactions.[5] This feature, together with the geometry of the membrane-binding interface, determines the ability of those domains to generate either membrane invaginations (BAR and most F-BAR), protrusions (I-BAR) or even stabilized planar membrane sheets (PinkBAR).[6] Curiously, the unique membrane-deforming activity of the latter protein derives from its flat lipid-binding interface and formation of sheet-like oligomers in crystals as well as in solution.[6c] Although huge effort has been put on identifying the general features responsible for curvature generation, the detailed description of the physicochemical origin of curvature induction is still missing. We try to fill this gap with a synthetic biology approach[7] using DNA origami nanostructures.

The DNA origami technique allows folding of long, single-stranded "scaffold" DNA into custom-shaped nanoscale objects by a large number of short "staple" oligonucleotides that bind to defined segments of the "scaffold" strand.[8] This enables to construct two-[8a] and three-dimensional arrays[9] of helical DNA structures with predesigned curvature or twist.[10] Moreover, each staple strand can be independently functionalized using various chemical groups, which allows precise three-dimensional placement of functional moieties[11] such as lipids or other hydrophobic compounds.[12] By using such anchors, several groups showed the ability of distinct DNA origami nanostructures to bind to lipid membranes.[13] Recently we created highly elongated DNA origami nanorods, which readily bind to lipid membranes using cholesteryl anchors and showed switchable liquid-ordered/liquid-disordered partitioning.[14] Selective fluorescent labeling and fluorescence correlation spectroscopy allowed to elicit the rotational and translational diffusion of the nanorods on the membrane. While increasing the density of the rods, an isotropic–nematic transition was observed.[15] Similar membrane-mediated self-organization of strongly elongated protein molecules into nematic domains is supposed to be the initial step of membrane shape transformation in cells.[16]

Here, we undertook the challenge to reconstruct molecular events leading to large-scale membrane deformation driven by the oligomerization of nanoscopic lipid bilayer-anchored molecules of defined geometry. Stiff 3D DNA origami platforms, mimicking the subunits of a flat sheet-like

[*] Dr. H. G. Franquelim, Prof. P. Schwille
Department of Cellular and Molecular Biophysics
Max Planck Institute of Biochemistry
Am Klopferspitz 18, 82152 Martinsried (Germany)
E-mail: schwille@biochem.mpg.de
Homepage: http://www.biochem.mpg.de/en/rd/schwille/
Dr. A. Czogalla
Biotechnology Center of the TU Dresden
Tatzberg 47/51, 01307 Dresden (Germany)
and
Department of Cytobiochemistry, Faculty of Biotechnology
University of Wrocław
ul. F. Joliot-Curie 14a, 50383 Wrocław (Poland)
D. J. Kauert, Prof. R. Seidel
Institute for Molecular Cell Biology, University of Münster
Schlossplatz 5, 48149 Münster (Germany)
Dr. V. Uzunova, Dr. Y. Zhang
B CUBE—Center for Molecular Bioengineering
Dresden, University of Technology
Arnoldstraße 18, 01307 Dresden (Germany)

[**] This work has been supported in collaborative research centers of the Deutsche Forschungsgemeinschaft (DFG), begun in TRR83, and continued in SFB863. H.G.F. acknowledges the receipt of a Humboldt Research Fellowship. Further support was given by the Max Planck Society to P.S., the Leibniz Association and the BMBF (grant numbers SAW-2011-IPF-2/380032 and 03Z2E511) to V.U. and Y.Z. as well as by the European Research Council (grant number GA 261224) and by the DFG (TRR61) to R.S.

Supporting information for this article is available on the WWW under http://dx.doi.org/10.1002/anie.201501173.

membrane-sculpting scaffold (Figure 1) were assessed to bind and deform model membranes. We introduced two units to better control the interactions between individual molecules and spatial arrangement of membrane-binding sites during oligomerization, which are critical factors in protein-assisted membrane deformation.

The 3D shape of our DNA origami platform resembles a monolith, with a lower flat facet of roughly 50 nm × 40 nm in size and a smaller top face (Figures 1 A–B and S1 in the Supporting Information). They were assembled as previously described[17] and their correct folding checked by transmission electron microscopy (TEM) imaging (Figure 1 C and Supporting Information). The structures contained three different functional modifications: i) nine cholesteryl–triethylene glycol (TEG) modified staples at the bottom side of the lower facet to promote binding to the membrane, ii) ten Alexa-Fluor-modified staples at the top facet (construct A with Alexa 488 and construct B with Alexa 647) to support fluorescence detection, and iii) six single-stranded overhangs (11 nucleotides each) at each of two opposing lateral sites (on each DNA monolith construct complementary lateral overhangs were introduced), which enables them to oligomerize as displayed in Figure 1 D. Individually, constructs A and B were not capable to self-oligomerize (Figures 1 C and S2); yet, in combination, they form highly ordered oligomers in solution (Figures 1 E and S2) that resemble a brick-like wall, where each brick layer is composed of one kind of structure. Analysis using gel electrophoresis further corroborates these findings (Figure S3).

We first started to visualize the binding of amphiphilic constructs A and B separately to giant unilamellar vesicles (GUVs) using fluorescence imaging and performed fluorescence correlation spectroscopy (FCS) measurements. Both constructs readily bind to free-standing lipid membranes and undergo Brownian motion on the membrane surface. At low surface densities (< 4 particles μm^{-2}) a value of $D = 2.5 \pm 0.2\ \mu m^2 s^{-1}$ was retrieved for the translational diffusion of both structures (Figures 2 and S5). Thus, the translational diffusion coefficient is about a factor 1.6 larger than the reported values for elongated DNA nanoneedles.[14,15]

Further on, we analyzed combined interaction and oligomerization of both constructs on model membranes at different surface density ranges. The diffusion coefficients measured by FCS (Figure S5) were substantially lower for the oligomerizing monoliths when compared to the non-interacting species. At intermediate DNA monolith surface densities (5 to 10 particles μm^{-2}), large immobile origami patches were observed by confocal imaging, the shapes of which were identical in both fluorescence channels. This suggests that construct A (in green) and B (in red) are equally present in these patches and are oligomerized into larger superstructures (Figure 3 A). This is in agreement with lateral interactions between individual DNA origami monoliths in the plane of the membrane, as expected from the multimerization design displayed in Figure 1 D. Similar partial vesicle coverage has been reported in reconstitution studies involving scaffold- and coat-forming proteins.[18]

The oligomerization of constructs A and B on free-standing membranes was also investigated at lower surface

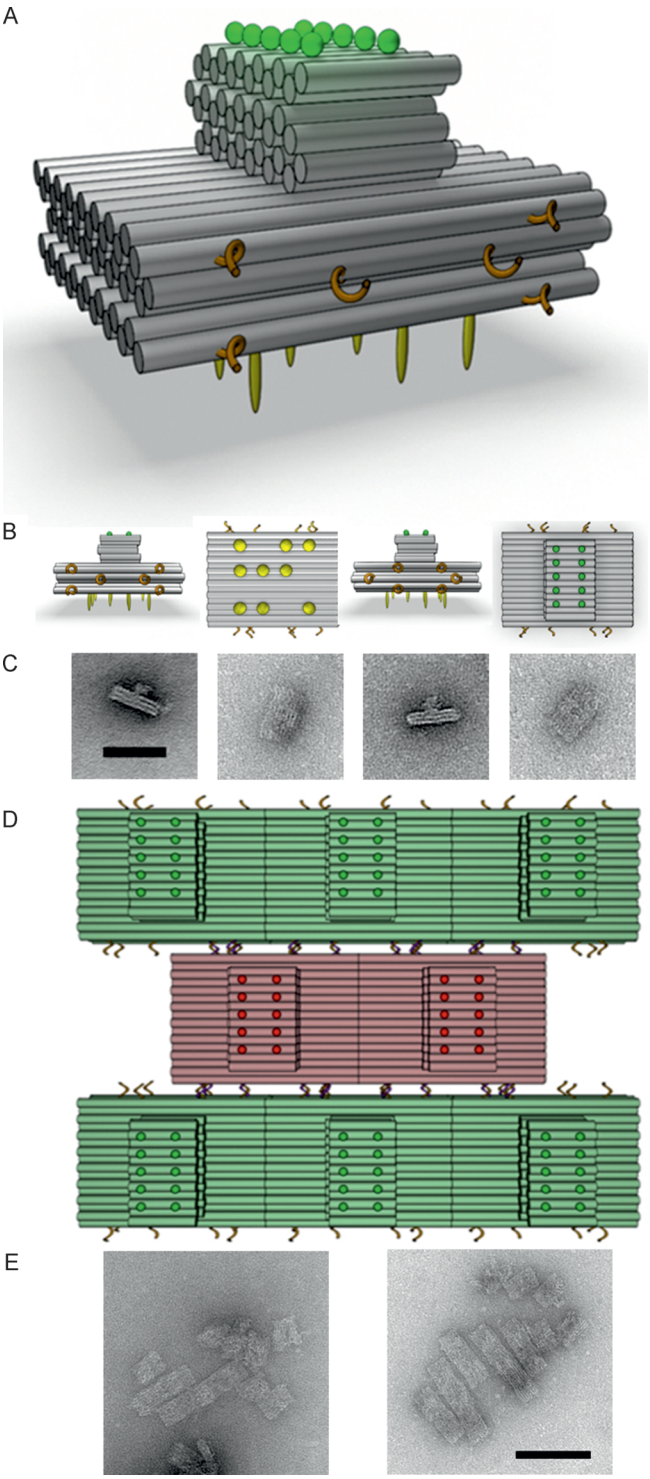

Figure 1. Amphipathic DNA origami monoliths. A–B) Schematics of helix bundle arrangement of the two structures (structure A) distinguished by attached fluorescent molecules (Alexa 488: green) and "sticky" oligonucleotide overhangs (orange). Cholesteryl-TEG anchors (yellow) are located at the surface opposite to fluorescent dyes. C) Representative TEM images of individual DNA origami structures (scale bar: 50 nm). D) After mixing construct A (green) and construct B (red) both structures interact with each other because of interactions of complementary "sticky" oligonucleotide overhangs. E) Representative TEM images of the resulted scaffolds (scale bar: 100 nm).

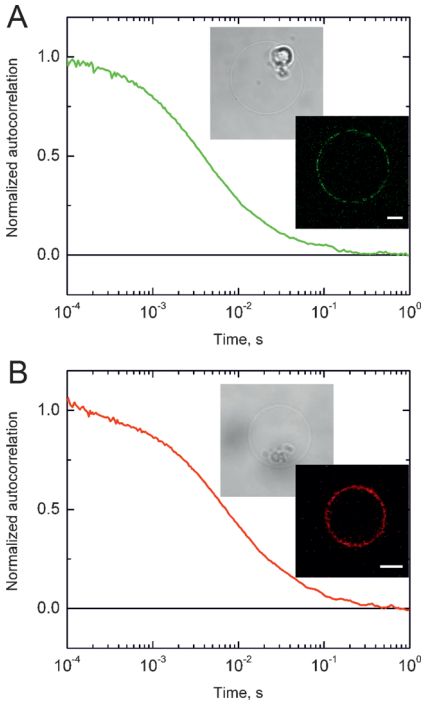

Figure 2. Origami DNA monoliths attached to free-standing membranes. Representative confocal images (transmitted light and fluorescence) of GUVs at low surface densities (<4 particles μm^{-2}) of origami DNA nanostructures together with representative normalized FCS autocorrelation curves (calculated diffusion coefficient, *D*, is $2{,}5 \pm 0{,}2\ \mu m^2 s^{-1}$) for construct A (A) and construct B (B). Scale bars: 10 μm.

densities (5.4 ± 1.3 particles μm^{-2}, 1 % of the membrane surface covered by the structures) using a quantitative dual-color fluorescence cross-correlation spectroscopy (FCCS) approach. Figure 3 B–C illustrates typical autocorrelation and cross-correlation curves for the combined interaction of constructs A and B on GUVs, but also of non-interacting analogs of A and B that lack the lateral oligonucleotide overhangs ($A^{(-)}$ and $B^{(-)}$). The increased cross-correlation amplitudes observed for constructs A and B, in combination, give evidence that they co-diffuse at the membrane interface, unlike the combination of $A^{(-)}$ and $B^{(-)}$. A detailed analysis of the full set of dual-color FCCS data enabled to calculate the average CC_{max} value (see the Supporting Information), which was $65\,\% \pm 13\,\%$ ($n = 6$) for the constructs with overhangs ($A + B$) and always below 20 % for constructs without overhangs ($A^{(-)} + B^{(-)}$). Thus, these results support the presence of nanoscale oligomers of constructs A and B on top of the model membranes. Moreover, the shape of the correlation curves for combined A and B constructs indicates the formation of higher-order oligomers reflected by large distortions of the curves at longer times (>0.1 s; Figure 3 B). Such contributions from slowly diffusing species are much less pronounced for membranes bearing $A^{(-)}$ and $B^{(-)}$ (Figure 3 C).

We next investigated whether constructs A and B in combination are able to scaffold giant vesicles at a larger scale. High DNA origami membrane surface densities (>10 particles μm^{-2}) resulted in full coverage of GUVs by

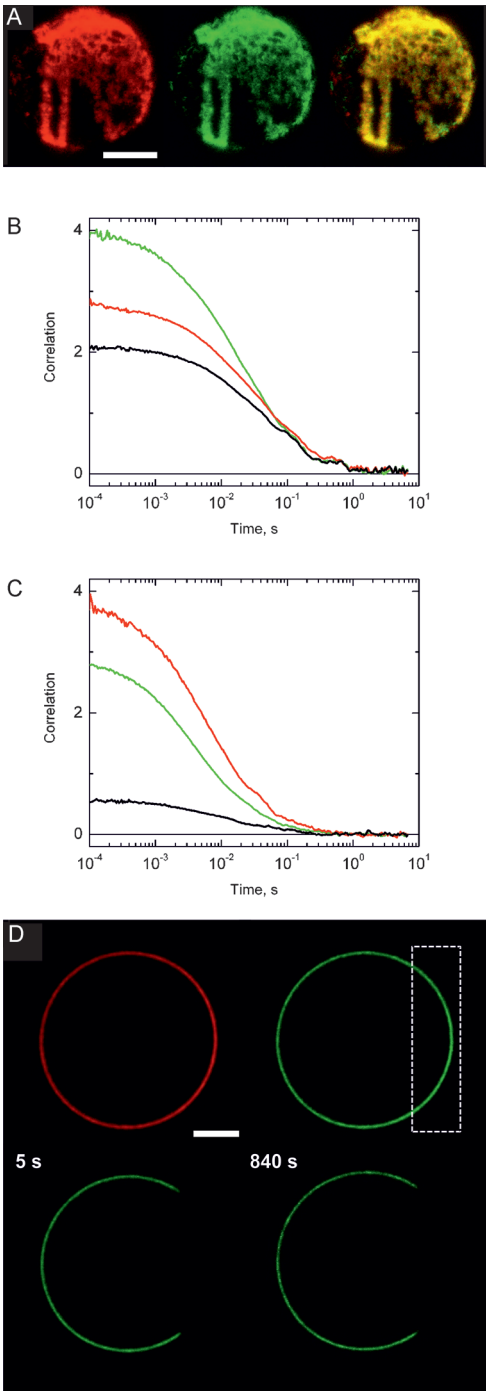

Figure 3. Oligomerization of origami DNA monoliths with "sticky" overhangs on free-standing membranes. A) Z-stack projection of the upper half of a GUV at intermediate surface densities of a mixture of constructs A and B, which results in a partially scaffolded membrane surface (left and central panel represent signal from constructs A and B, respectively; right: merged channels). B) Representative FCCS curves for mixed constructs A + B at low (approximately 5 particles μm^{-2}) membrane surface densities. C) FCCS curves for mixed non-interacting constructs $A^{(-)}$ and $B^{(-)}$, which lack sticky oligonucleotide overhangs, at comparable surface densities. FCCS curves are in black. D) FRAP of a GUV fully covered with oligomerizing constructs A and B at equatorial plane, only the green channel (construct A) was bleached (dashed rectangle), the red channel is construct B. Scale bars: 10 μm.

both of our nanostructures. The formation of a compact 2D lattice of DNA origami was indicated by a qualitative fluorescence recovery after photobleaching (FRAP; Figure 3D). In analogy to recent evidence of the reduced mobility of several membrane-sculpting BAR proteins on membranes[19] as well as lateral crosslink of proteins during assembly of the autophagosomal membrane coat,[18a] limited fluorescence recovery of the combined membrane-bound oligomerizable DNA nanostructures was detectable. This is in agreement with the decrease in mobility reported in Figure S5. Thus, the monoliths form a dense immobile layer on top of the free-standing membranes indicating subunit oligomerization and the formation of a rigid lattice of DNA origami monoliths scaffolding the GUV. Notably, diffusion of fluorescent lipid analogs (i.e. DiD) within the covered membranes is not affected by the cholesteryl-TEG-anchored DNA origami structures, as shown previously.[14]

To finally test whether the proposed synthetic approach ultimately can lead to membrane deformations as they are observed for biological peripheral membrane protein scaffolds, we evaluated the shapes of GUVs at high membrane surface densities of our DNA origami constructs. In the absence of DNA monoliths, nearly all vesicles were spherical in shape (Figures 4 and S4). Similar results were obtained for GUVs covered with constructs $A^{(-)}$ and $B^{(-)}$ (without lateral overhangs). Interestingly, in the presence of constructs A and B (having lateral complementary overhangs), for which the subunits are able to self-oligomerize in the lateral direction, more than half of the vesicles assumed non-spherical shapes, typically characterized by planar deformations (Figures 4B–D and S4; Figure 3D depicts GUVs belonging to the non-deformed spherical subset). The coverage of the membrane surface by our structures (>10 particles μm^{-2}, membrane-binding area per single molecule of approximately 2000 nm^2) in this experiment is similar to coverages of amphiphysin BAR domain (>1000 particles μm^{-2}, membrane-binding area per amphiphysin dimer of approximately 45 nm^2, PDB: 4ATM) that are required to deform GUVs.[4] Crowding effects[20] cannot be the sole justification, since the deformation is correlated with the presence of interactions between A and B monomers (Figure 4C). Similar planar deformations on model membranes have been documented for the flat PinkBAR domain,[6c] the F-BAR protein Nervous Wreck,[21] the autophagosomal coat complex,[18a] and two-dimensional streptavidin crystals.[22] There, the scaffolding subunits were capable of building large lattices on lipid bilayers, analogous to what we report for a mixture of constructs A and B. A distinct property of the vesicles that were deformed by the oligomerizing constructs A and B is that they were much more resistant to spontaneous collapse at the bottom of the observation chamber as most of them survive for 3–5 days instead of collapsing after one day as observed for GUVs with the non-interacting DNA origami constructs. Furthermore, the form of the membrane deformations observed here can be correlated with the shape of the individual DNA origami subunits, as described for PinkBAR domains.[6c] Though the individual oligonucleotide bridges between structures A and B may be rather flexible, the overall 2D assembly is likely

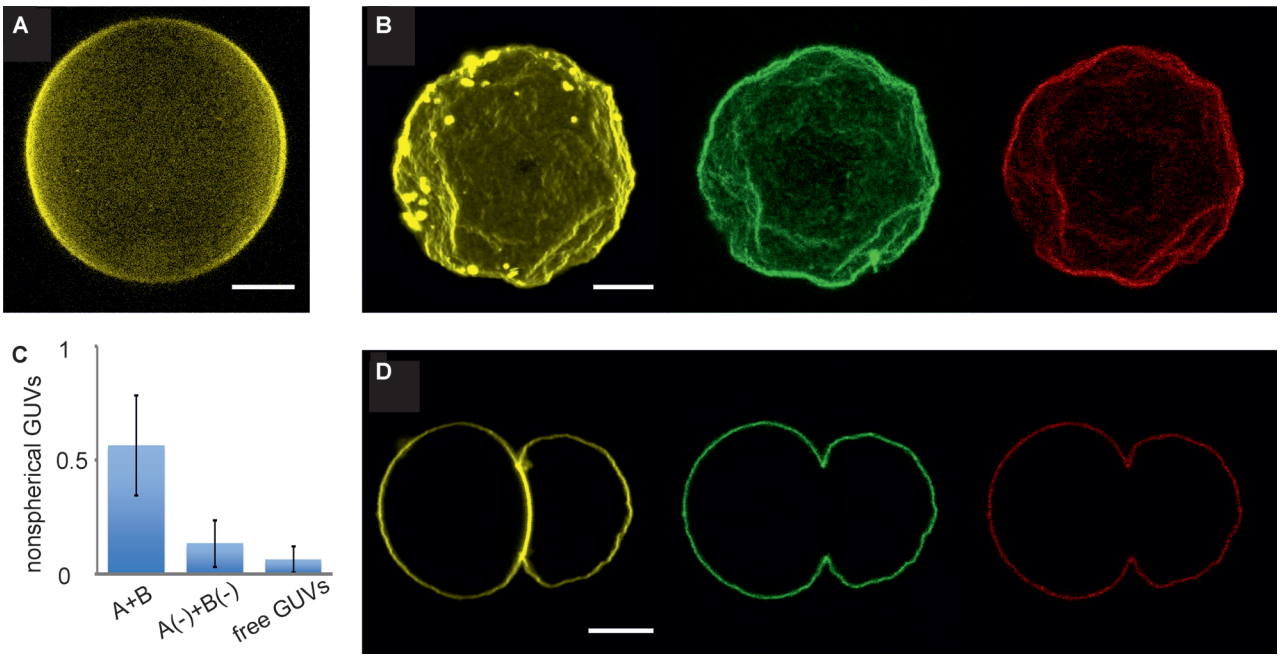

Figure 4. Oligomerization-driven deformation of membranes induced at high surface densities of origami DNA monoliths with "sticky" overhangs. A) 3D reconstruction of a GUV without origami DNA on its surface. A similar morphology was observed for GUVs bearing constructs $A^{(-)}$ and $B^{(-)}$ lacking "sticky" oligonucleotide overhangs. B) 3D morphology and D) confocal projection in the equatorial plane of a GUV scaffolded with constructs A and B, both with "sticky" overhangs, at surface densities $\geqslant 10$ particles μm^{-2}. C) Quantification of the ratio of deformed GUVs (for A + B $n = 54$; for $A^{(-)} + B^{(-)}$ $n = 50$; for bare vesicles $n = 82$). The yellow channel represents membrane labeled with the fluorescent lipid analog DiI; green: construct A and red: construct B. Scale bars: 10 μm.

very stable, which may arise from the large number of oligonucleotide bridges at the monolith sites and stacking interactions between structures at the DNA helix ends. The DNA monoliths bind to lipid membranes from their flat side (Figure 1) and their concerted lateral oligomerization supports a two-dimensional planar arrangement, which interferes with the shape of the membrane deformations. The importance of these structural features during membrane remodeling has been, for example, extensively addressed to describe the mode of action of several protein membrane coats.[1b,3,23]

In conclusion, we built a synthetic DNA scaffold capable of membrane sculpting. It is based on two versions of a planar 3D DNA origami structure that were able to attach to membranes and undergo planar multimerization when added together. Only DNA origami monomers that laterally bind to neighboring monomers were shown to co-localize and co-diffuse on top of giant vesicles. At high surface densities, those constructs formed a scaffold and even promoted extensive planar deformations, according to the flat geometry of the DNA origami membrane-binding interface and the 2D coordination of lattice formation. A similar concerted molecular mechanism based on self-assembly of subunits has been generally assumed to trigger membrane deformations by BAR domains,[5,24] other scaffolding elements,[18] and even viral proteins.[25] Our work mainly focused on mimicking the oligomerization steps of biological membrane scaffolding proteins that drive the membrane deformations, which is a basis to explore the importance of physicochemical properties of scaffolding proteins. However, a more detailed view of such properties requires design of curved DNA structures, ideally with molecular shapes and dimensions resembling those known from scaffolding proteins. Another challenging task is to reconstitute into DNA origami nanostructures the mixed charge–charge/hydrophobic mode of membrane interactions known from those proteins.

Keywords: diffusion · lipid membranes · membrane deformation · oligomerization · origami DNA structures

How to cite: *Angew. Chem. Int. Ed.* **2015**, *54*, 6501 – 6505
Angew. Chem. **2015**, *127*, 6601 – 6605

[1] a) K. Farsad, P. De Camilli, *Curr. Opin. Cell Biol.* **2003**, *15*, 372 – 381; b) M. M. Kozlov, F. Campelo, N. Liska, L. V. Chernomordik, S. J. Marrink, H. T. McMahon, *Curr. Opin. Cell Biol.* **2014**, *29*, 53 – 60.
[2] a) A. Frost, V. M. Unger, P. De Camilli, *Cell* **2009**, *137*, 191 – 196; b) O. Daumke, A. Roux, V. Haucke, *Cell* **2014**, *156*, 882 – 892.
[3] H. T. McMahon, J. L. Gallop, *Nature* **2005**, *438*, 590 – 596.
[4] B. Sorre, A. Callan-Jones, J. Manzi, B. Goud, J. Prost, P. Bassereau, A. Roux, *Proc. Natl. Acad. Sci. USA* **2012**, *109*, 173 – 178.
[5] A. Frost, R. Perera, A. Roux, K. Spasov, O. Destaing, E. H. Egelman, P. De Camilli, V. M. Unger, *Cell* **2008**, *132*, 807 – 817.
[6] a) B. Qualmann, D. Koch, M. M. Kessels, *EMBO J.* **2011**, *30*, 3501 – 3515; b) H. Zhao, A. Pykalainen, P. Lappalainen, *Curr. Opin. Cell Biol.* **2011**, *23*, 14 – 21; c) A. Pykäläinen, M. Boczkowska, H. Zhao, J. Saarikangas, G. Rebowski, M. Jansen, J. Hakanen, E. V. Koskela, J. Peranen, H. Vihinen, E. Jokitalo, M. Salminen, E. Ikonen, R. Dominguez, P. Lappalainen, *Nat. Struct. Mol. Biol.* **2011**, *18*, 902 – 907.
[7] P. Schwille, *Science* **2011**, *333*, 1252 – 1254.
[8] a) P. W. Rothemund, *Nature* **2006**, *440*, 297 – 302; b) C. E. Castro, F. Kilchherr, D. N. Kim, E. L. Shiao, T. Wauer, P. Wortmann, M. Bathe, H. Dietz, *Nat. Methods* **2011**, *8*, 221 – 229.
[9] S. M. Douglas, H. Dietz, T. Liedl, B. Hogberg, F. Graf, W. M. Shih, *Nature* **2009**, *459*, 414 – 418.
[10] H. Dietz, S. M. Douglas, W. M. Shih, *Science* **2009**, *325*, 725 – 730.
[11] a) K. Jahn, T. Torring, N. V. Voigt, R. S. Sorensen, A. L. Bank Kodal, E. S. Andersen, K. V. Gothelf, J. Kjems, *Bioconjugate Chem.* **2011**, *22*, 819 – 823; b) F. C. Simmel, *Curr. Opin. Biotechnol.* **2012**, *23*, 516 – 521.
[12] M. Schade, D. Berti, D. Huster, A. Herrmann, A. Arbuzova, *Adv. Colloid Interface Sci.* **2014**, *208*, 235 – 251.
[13] a) M. Langecker, V. Arnaut, T. G. Martin, J. List, S. Renner, M. Mayer, H. Dietz, F. C. Simmel, *Science* **2012**, *338*, 932 – 936; b) S. D. Perrault, W. M. Shih, *ACS Nano* **2014**, *8*, 5132 – 5140; c) Y. Suzuki, M. Endo, Y. Yang, H. Sugiyama, *J. Am. Chem. Soc.* **2014**, *136*, 1714 – 1717; d) J. R. Burns, K. Gopfrich, J. W. Wood, V. V. Thacker, E. Stulz, U. F. Keyser, S. Howorka, *Angew. Chem. Int. Ed.* **2013**, *52*, 12069 – 12072; *Angew. Chem.* **2013**, *125*, 12291 – 12294.
[14] A. Czogalla, E. P. Petrov, D. J. Kauert, V. Uzunova, Y. Zhang, R. Seidel, P. Schwille, *Faraday Discuss.* **2013**, *161*, 31 – 43; discussion 113 – 150.
[15] A. Czogalla, D. J. Kauert, R. Seidel, P. Schwille, E. P. Petrov, *Nano Lett.* **2015**, *15*, 649 – 655.
[16] a) N. Ramakrishnan, P. B. Sunil Kumar, J. H. Ipsen, *Biophys. J.* **2013**, *104*, 1018 – 1028; b) M. Simunovic, C. Mim, T. C. Marlovits, G. Resch, V. M. Unger, G. A. Voth, *Biophys. J.* **2013**, *105*, 711 – 719.
[17] D. J. Kauert, T. Kurth, T. Liedl, R. Seidel, *Nano Lett.* **2011**, *11*, 5558 – 5563.
[18] a) A. Kaufmann, V. Beier, H. G. Franquelim, T. Wollert, *Cell* **2014**, *156*, 469 – 481; b) J. B. Manneville, J. F. Casella, E. Ambroggio, P. Gounon, J. Bertherat, P. Bassereau, J. Cartaud, B. Antonny, B. Goud, *Proc. Natl. Acad. Sci. USA* **2008**, *105*, 16946 – 16951.
[19] H. Zhao, A. Michelot, E. V. Koskela, V. Tkach, D. Stamou, D. G. Drubin, P. Lappalainen, *Cell Rep.* **2013**, *4*, 1213 – 1223.
[20] J. C. Stachowiak, E. M. Schmid, C. J. Ryan, H. S. Ann, D. Y. Sasaki, M. B. Sherman, P. L. Geissler, D. A. Fletcher, C. C. Hayden, *Nat. Cell Biol.* **2012**, *14*, 944 – 949.
[21] A. N. Becalska, C. F. Kelley, C. Berciu, T. B. Stanishneva-Konovalova, X. Fu, S. Wang, O. S. Sokolova, D. Nicastro, A. A. Rodal, *Mol. Biol. Cell* **2013**, *24*, 2406 – 2418.
[22] M. R. Horton, S. Manley, S. R. Arevalo, A. E. Lobkovsky, A. P. Gast, *J. Phys. Chem. B* **2007**, *111*, 880 – 885.
[23] a) B. Antonny, *Curr. Opin. Cell Biol.* **2006**, *18*, 386 – 394; b) P. Sens, L. Johannes, P. Bassereau, *Curr. Opin. Cell Biol.* **2008**, *20*, 476 – 482.
[24] H. Yu, K. Schulten, *PLoS Comput. Biol.* **2013**, *9*, e1002892.
[25] a) H. Ewers, W. Romer, A. E. Smith, K. Bacia, S. Dmitrieff, W. Chai, R. Mancini, J. Kartenbeck, V. Chambon, L. Berland, A. Oppenheim, G. Schwarzmann, T. Feizi, P. Schwille, P. Sens, A. Helenius, L. Johannes, *Nat. Cell Biol.* **2010**, *12*, 11 – 18; sup pp. 11 – 12; b) A. V. Shnyrova, J. Ayllon, I. I. Mikhalyov, E. Villar, J. Zimmerberg, V. A. Frolov, *J. Cell Biol.* **2007**, *179*, 627 – 633; c) J. Solon, O. Gareil, P. Bassereau, Y. Gaudin, *J. Gen. Virol.* **2005**, *86*, 3357 – 3363.

Received: February 6, 2015
Revised: March 13, 2015
Published online: April 16, 2015

